Article

Satellite to Ground Station, Attenuation Prediction for 2.4-72GHz using LTSM, an artificial recurrent neural network technology

Menachem Domb [1], Guy Leshem[1]

[1] Computer Science Department, Ashkelon Academy College (AAC), Ashkelon, Israel

* Correspondence: dombmnc@edu.aac.ac.il;

Abstract: Free-space communication is a leading component in global communications. Its advantages relate to a broader signal spread, no wiring, and ease of engagement. Satellite communication services became recently attractive to mega-companies that foresee an excellent opportunity to connect disconnected remote regions, serve emerging machine-to-machine communication, Internet-of-things connectivity, and more. Satellite communication links suffer from arbitrary weather phenomena such as clouds, rain, snow, fog, and dust. In addition, when signals approach the ground station, it has to overcome buildings blocking the direct access to the ground station. Therefore, satellites commonly use redundant signal strength to ensure constant and continuous signal transmission, resulting in excess energy consumption, challenging the limited power capacity generated by solar energy or the fixed amount of fuel. This research proposes LTSM, an artificial recurrent neural network technology that provides a time-dependent prediction of the expected attenuation level due to rain and fog and the signal strength that remained after crossing physical obstacles surrounding the ground station. The satellite transmitter is calibrated accordingly. The satellite outgoing signal strength is based on the predicted signal strength to ensure it will remain strong enough for the ground station to process it. The instant calibration eliminates the excess use of energy resulting in energy savings.

Keywords: Satellite Communication, Signal Propagation, Rain Attenuation, Urban area ground station, SNR, ITU-R, LSTM, Neural network

1. Introduction

During the recent two decades, cellular wireless infrastructure has served as the standard data transmission system. However, the expected growing demand for internet services, high speed, wide bandwidth, and availability requires a significant change in communication infrastructure, deployment, technology, and management. Free space high-speed communications, employing numerous satellites and related ground stations, seem to reasonably fulfill this extreme demand.

Higher frequencies are considerably affected by rainfall that attenuates the propagating signal at microwave and millimeter-wave frequencies. Therefore, mitigating rain attenuation is required to ensure the quality of microwave and millimeter-wave links. Dynamic attenuation mitigation methods are implemented alongside attenuation prediction models. Calculating the impact of rain on satellite communication relies on attenuation data collected for each ground station and transmission frequency. This data, together with standard prediction methods, enables us to estimate the expected attenuation per location. The availability of satellite beacon measurements has provided a database for validating and refining the prediction models. The predicting methods recommended by

Preprints (www.preprints.org) | NOT PEER-REVIEWED | Posted: 2 December 2021 doi:10.20944/preprints202112.0031.v1

the ITU-R assume that an equivalent cell of uniform rainfall rate can model the non-uniform rainfall along the propagation path. An identical cylindrical cell of constant rain can intercept the link at any position with equal probability. A practical path length is calculated as the average length of the intersection between the cell and the propagation path. As a result, the effective path length is always smaller than the actual path length. In the slant path prediction method, horizontal and vertical reduction factors consider the spatial and temporal variability of the rain field.

A satellite cruises in a specific orbit while receiving and sending signals to and from a ground station. The ground station is located in a fixed location. Figure 1 depicts the entire scene where the ground station, satellite, and orbit are synchronized to enable data transmission between them. The signal route from the satellite to the ground station contains two sections, designated as A and B in Figure 1. Section A focuses on predicting the attenuation level of signals from the satellite, passing the free space up to the ground buildings. Section B indicates the remaining signal strength after it passes the blocking buildings surrounding the ground station. Sections A and B complement each other to predict the initial signal strength by satellite to overcome the accumulated signal attenuation when passing both sections.

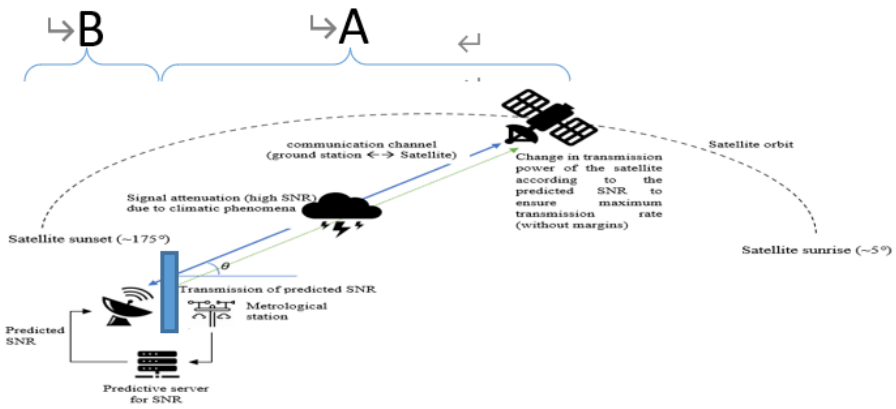

Figure 1: The satellite communication setup

The satellite Link Budget, *LB*, is distributed among the panels, including the P_T transmitter output power (dBm), G_T transmitter antenna gain (*dBi*), G_R receiver antenna gain (*dBi*), L_{FS} free-space propagation loss, and L_M ($=L_S+L_R$) miscellaneous losses (fading margin, body loss, polarization mismatch, and other losses) (dB). The link budget can be expressed as $LB = P_T + G_T + G_R + L_{FS} + L_M$. and $\text{SNR}=\frac{PT \cdot GT \cdot GR \cdot LFS \cdot LM}{N_0 \cdot B}$ Where N_0 is the basic noise level and B is the signal bandwidth. To maintain an SNR that ensures the maximum transmission rate when the signal attenuation changes (L_M decreases or increases), the transmission output power P_T is changed accordingly. Figure 2 depicts the components used for calculating the *LB* value. We used the STK simulator to obtain synthetic communication data between the satellite and the ground station according to different weather-situation data to prove our approach.

Typical ground stations in modern urban areas are surrounded by high buildings disturbing the propagation of electromagnetic waves. We focus on the reflections and diffractions signals caused by structures, leading to reduced signal effectiveness and signal loss.

The combination of predicting the signal attenuation and performing the correction of the transmission intensities make it possible to maintain proper Signal-to-Noise Ratio (SNR) and prevent transmission interference. For each section, A and B, we have developed a separate prediction model using LSTM and an associated Python programming software. We used collected data from the Genesis LEO satellite and corresponding simulated data in the range of 2.4GHz to 72GHz. We then executed two LSTM systems, one for each section, to predict the attenuation levels in each part. We reached less than a 2% gap between the predicted and the actual attenuation levels for each piece. We calculated the expected SNR based on this data, the ITU model, and the LSTM neural networks for

Preprints (www.preprints.org) | NOT PEER-REVIEWED | Posted: 2 December 2021 doi:10.20944/preprints202112.0031.v1

a few seconds ahead. Based on the predicted SNRs, the signal strength is changed accordingly, resulting in reduced power consumption. We conducted separate experiments for each frequency. Results show that the predicted measurements for all frequencies are very close to the actual value.

The rest of this paper is organized as follows: section 2 outlines related work, section 3 presents our model for predicting the signal attenuation level due to climate situations and blocking construction near the ground station, section 4 outlines the experiment setup and the corresponding results for each route section, and in section 5 we conclude with conclusions and future work. Where applicable, we separated between sections A and B to emphasize the differences.

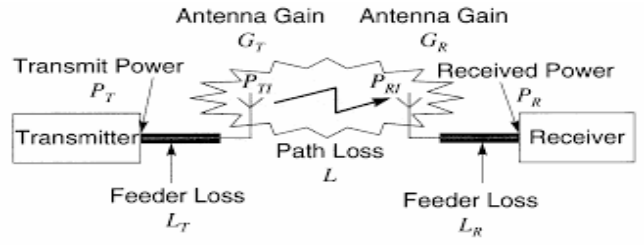

Figure 2: The components used for calculating the LB value

2. Related Work

Section A:

Samad et al. [1] provide a comprehensive overview of past and current rain attenuation models outlining *classification*, accuracy, and comparison with additional details on the LA rain attenuation (LARA) models. Kalaivaanan et al. [2] suggest antennas with a larger diameter to receive a broader range of data that improves the accuracy of the results and reduces the rain attenuation prediction error. They used a Ka-band with an antenna with a diameter of above 7.2m in tropical regions to prove this. Dahman et al. [3] propose a binary decision probabilistic method for Ka frequency rain attenuation forecast using a predetermined threshold. It is a known protocol adjusted for probabilistic weather forecasts in a communication satellite control loop. Golovachev et al. [4] show the reduction of the bit error rate for the orthogonal frequency-division multiplexing (OFDM) communication link applied for millimeter waves (MMW, 30-300 GHz) transmission. Bonev et al. [5] analyzed rain attenuation measurements collected over four years, working at 11,15 and 19 GHz, and proposed to improve the rain-prediction model's accuracy coefficients. Bundall et al. [6], who focus on the distance factor for MMW links, found that the distance values for the path lengths up to 1 km are inconsistent. They propose a fix for the distance factor in ITU-R P530.17. P Through [7] based its measurement of multiple antenna sizes.

Yeo et al. [8] present a rain attenuation model for the *tropical* region with a rainfall rate of 0.01% at the time. It collects input from two satellites operating at Ka-band (WINDS) and Ku-band (GE23), 18.9 and 12.75 GHz, respectively. The gap between the predicted and the actual measures shows that the gap is less than those predicted by the ITU-R, Yamada, DAH, Karasawa, and Ramachandran models. Islam et al. [9] propose an improvement of ITU-R for tropical regions and 15GHz frequency. Ahuna et al. [10] offer a combination of rainfall statistics and an ML-based model, which uses a neural network trained by rainfall data collected in South Africa for four years. They found that the gap between the predicted and actual results was close, which is better than other models for short sampling time. Das et al. [11] noticed that a rainfall prediction model applied for tropical regions does not generate the same accuracy when applied to other areas. A proper μ and s model is required to fit other locations, assuming that a large data set exists for the desired region at different frequencies. Hence, a global model for μ and s is applicable for any area for a time series of rain attenuation. Fadilah and Pratama [12] compared rain attenuation prediction in Indonesia using the ITU-R, Global Crane, and DAH models. The study concludes that ITU-R provides the closest forecast.

Preprints (www.preprints.org) | NOT PEER-REVIEWED | Posted: 2 December 2021 doi:10.20944/preprints202112.0031.v1

Most of the reviewed models relate to the tropical region while ignoring others. Sakir and Atiqul [13] used I areas of Bangladesh using 36 to 46 GHz and V 46 to 56 GHz bands. They observed that the attenuation varies from 40 dB to 170 dB, which is relatively high. Hence, maintaining the connection for 99.99% of the rainy season requires 140 dB and 100 dB, respectively. They explored methods to improve the performance and the accuracy of the SNR prediction for LTE and 5G, Wireless Networks and Mobile Communications. They achieved less than 1 ms process time and complete accuracy when utilizing time-domain signals for SNR range of [-4, 32] dB and resolution of 2 dB. P. Kazemi et al. [15] proposed an algorithm for improving the handover decisions between two BS, eliminating UE assistance and HO reduction. They used ML to predict the SNR of transmissions between two 5G cellular base stations. S.H.A. Shah et al. [16] propose an LSTM-based system for predicting multi-directional link quality in mm-Wave systems in wireless systems. It simulated multi-cell link and vehicular blockers at 28 and 140 GHz and beamed prediction in an indoor setting at 60 GHz.

Tozer et al. [17] Outline the application and features of High-Altitude Platforms (HAP) to deliver future broadband wireless communications. The term building entry loss we used here corresponds to the definition made at ITU-R Rec. [17], defined as the excess loss due to building walls and other building features. Building entry loss depends on the building type, construction, and electrical parameters of the material used. Measurements of Penetration loss of various building materials at 1–8 GHz appear in [18]. [19,20] present electrical parameters of materials of S-band frequencies. Many other aspects influence the building entry loss, such as the receiver's position inside the building, the transmitter, and so forth, making it difficult to accurately estimate the level of received power inside a building. A decrease of the entry losses into building with floor height can often be observed [21,22]. Entry loss measurements for 2 GHz are reported in [23,24]. Measuring the spread of the received signal within buildings has been reported in [25,26,27]. In [28], the authors focused on the overall building entry loss and building entry loss as a function of elevation and entry angle and the results of time delay spread. [29,30] presented a new model of the path loss parameters. D. Micheli et al. [31] describe a simple way to measure electric wave attenuation within an indoor scenario, demonstrating attenuation level differences for different wall materials and textures. Al-Hourani et al. [32] propose a framework for modeling satellite-to-ground signal attenuation in urban environments. It captures the shadowing using measurements collected from a global navigation satellite system (GNSS). The mentioned methods are based on various data analysis methods to identify the contributing parameters to signal loss. This approach requires proof of the truth of the found parameters. Our proposed system is based on accumulated data processed by proven ML methodologies generating improved and accurate outcomes.

In summary, for section A we reviewed rain attenuation and related prediction models. Some focus on a specific range of frequencies, particular world regions, or wireless systems but do not provide a comprehensive approach covering a broader frequency range or models independent of a specific area. For section B, we reviewed several proposals dependent on particular setups. This work proposes a general prediction model that can be adjusted to comply with any region and a broad spectrum of frequencies.

3. PredictiNG the Signal attenuation LEVEL

Section A: The proposed solution comprises three steps: a collection of SNR and weather conditions, collection of the attenuation levels, and application of the prediction model.

Collecting the SNR and weather conditions

In the first stage, we collect data on the SNR and weather conditions. Figure 3 depicts an example of the SNR station in December 2019.

Preprints (www.preprints.org) | NOT PEER-REVIEWED | Posted: 2 December 2021 doi:10.20944/preprints202112.0031.v1

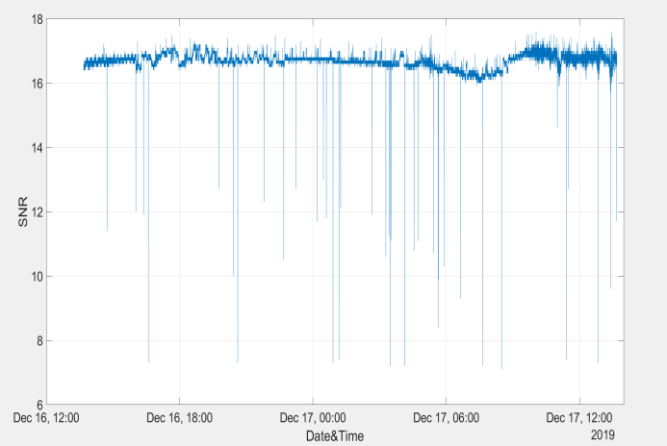

Figure 3. SNR Measurements Collection of the attenuation levels.

In stage 2, we collect the attenuation levels during the satellite transition in orbit for 24 hours. Figure 4 illustrates the various measurements and the attenuation level over the satellite orbit. It corresponds to the angle (θ) between the ground station and the satellite position.

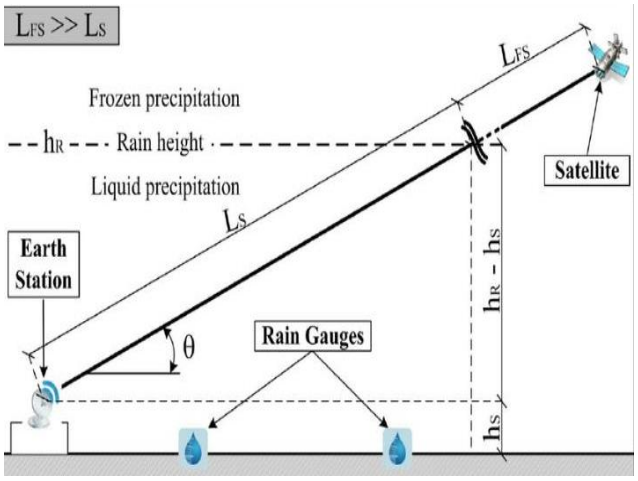

Figure 4. Various measurements and the attenuation level.

Application of the prediction model

In stage 3, we use ITU models to calculate channel damping due to climatic phenomena (clouds, rain, snow, etc.). The ITU-R method uses the concept of a sufficient path length using a reduction factor. The process calculates the long-term statistics of the slant path rain attenuation at a given location for frequencies up to 30GHz and provisionally for higher frequencies. This method involves several steps.

Building the database for the learner

We use the collected data related to SNR, climatic conditions, and satellite orbits to comprise a learner database to enable SNR prediction. We used data from 3 sources: STK simulation linking satellite orbit (time and angle) with channel orientation, weather data from a meteorological database, and SNR data measured by the satellite. Each record in the learner database represents an alignment of these three data sources. The record layout is sampling date and time, angle, temperature, frequency, humidity, bandwidths, and an indication of the passed or lost signal. Table 1 presents examples of the database used for training the deep learning system.

Preprints (www.preprints.org) | NOT PEER-REVIEWED | Posted: 2 December 2021 doi:10.20944/preprints202112.0031.v1

EXAMPLE OF THE TRAINING DATABASE

Index	Date	Time (UTCG)	Angle (dgrees)	Temperature (°C)	Relative humidity(%)	Rcvd. Frequency (GHz)	Bandwidth (kHz)	Rain Loss (dB)
0	4/10/2020	33:48.8	5.00	16.80	72.00	23.000491	32000	1.00
1	4/10/2020	33:49.0	5.39	16.90	73.00	23.000491	32000	1.00
2	4/10/2020	33:50.0	5.79	16.90	73.00	23.000491	32000	1.00
3	4/10/2020	33:51.0	6.18	16.90	73.00	23.000491	32000	1.00
4	4/10/2020	33:52.0	6.57	17.00	72.00	23.000491	32000	1.00
5	4/10/2020	33:53.0	6.97	16.90	72.00	23.000491	32000	1.00
6	4/10/2020	33:54.0	7.36	16.90	72.00	23.000491	32000	1.00
7	4/10/2020	33:55.0	7.75	16.80	73.00	23.000491	32000	1.00
8	4/10/2020	33:56.0	8.15	16.90	73.00	23.000491	32000	1.00
9	4/10/2020	33:57.0	8.54	16.90	74.00	23.000491	32000	1.00
10	4/10/2020	33:58.0	8.93	16.90	74.00	23.000491	32000	1.00
11	4/10/2020	33:59.0	9.33	16.90	74.00	23.000491	32000	1.00
12	4/10/2020	34:00.0	9.72	16.80	74.00	23.000491	32000	1.00
13	4/10/2020	34:01.0	10.11	16.70	73.00	23.000491	32000	1.00
14	4/10/2020	34:02.0	10.51	16.70	74.00	23.000491	32000	0.00
15	4/10/2020	34:03.0	10.90	16.70	75.00	23.00049	32000	0.00

Developing the predictive models

For the prediction method, we use a deep-learning algorithm that follows the following steps:

1. *Accept the training and testing dataset* - Table 1 is an example of the training and testing data set required to input the predicting system.
2. *Execute the prediction deep learning algorithm* - The input and output of the prediction procedure:

$$X_{m\times n,d,t} \rightarrow Y_{m^*\times 1,d,t+\Delta t}\ (train\ file)$$

$$\circledcirc\circledcirc\circledcirc\ X_{\tilde{m}\times n,d^*,t} \rightarrow Y_{\tilde{m}^*\times 1,d^*,t+\Delta t}\ (Test\ file)\ \circledcirc\circledcirc\circledcirc$$

In this section, we denote $X_{m\times n,d,t}$ a dataset of size m with n features, collected on day d and at time t. $Y_{m\times 1,d,t}$ is the class labels associated with $X_{m\times n,d,t}$. Therefore, the and Δt define a time variation given a dataset $X_{m\times n,d,t}$ known for d and t.

The following four steps comprise the proposed estimation procedure

Collect two samples of data, $X_{m\times n,d,t}$ and $X_{m\times n,d,t+\Delta t}$, $\Delta t > 0$,

Compute a new training set $Z_{m\times n+1,d}$, using $X_{m\times n,d,t}$ and $Y_{m\times 1,d,t+\Delta t}$ by concatenation, that is $Z_{m\times n+1,d} = [X_{m\times v,d,t}; Y_{m\times 1,d,t+\Delta t}]$,

Collect the test set $X_{\tilde{m}\times n,d+\Delta d,t}$ ($\Delta d > 0$), and compute $Y_{\tilde{m}\times 1,d+\Delta d,t+\Delta t}$ using the machine learning algorithm on $Z_{m\times n+1,d}$ and $X_{\tilde{m}\times n,d+\Delta d,t}$.

Training the learning system that predicts the channel attenuation

In this stage, we train the learning system. We use the LSTM model, an artificial neural network designed to recognize patterns in data sequences, such as numerical time series data emanating from neural networks as they have a temporal dimension. We use Matlab libraries to execute the LSTM. Below is the Matlab code:

```
clc
clear all
close all
session1_DataTrain=xlsread('DataTrain_10GHz.csv',1,'A1:G590')';
normalizedData=normalize(session1_DataTrain);
session2=xlsread('session2_10Ghz.csv',1,'A1:G585')';
normalized_Session2=normalize(session2);
session3=xlsread('session3_10GHz.csv',1,'A1:G506')';
normalized_Session3=normalize(session3);
```

Preprints (www.preprints.org) | NOT PEER-REVIEWED | Posted: 2 December 2021 doi:10.20944/preprints202112.0031.v1

```
output=xlsread('DataTrain_10GHz.csv',1,'H1:I590')';
% import normalized data+sessions+output
numFeatures = 7;
numHiddenUnits1 = 100;
numClasess = 2;
%define the architecture of the neural network
layers = [sequenceInputLayer(numFeatures),lstmLayer(numHiddenUnits1),fullyConnectedLayer(numClasess),regressionLayer]
;
%define the LSTM network
options = trainingOptions('adam', ...
    'MaxEpochs',250, ...
    'GradientThreshold',1, ...
    'InitialLearnRate',0.005, ...
    'LearnRateSchedule','piecewise', ...
    'LearnRateDropPeriod',125, ...
    'LearnRateDropFactor',0.2, ...
    'Verbose',0, ...
    'Plots','training-progress');
%define the optimizer and learning rate
net=trainNetwork(normalizedData,output,layers,options);
%save the model
outputPrediction_For_Session2=predict(net,normalized_Session2)';
outputPrediction_For_Session3=predict(net,normalized_Session3)';
```

Developing a model that ensures the maximum transmission rate

The ground station sends the predicted SNR to the satellite. We use the following model to maintain a constant SNR, which may be different from the expected SNR.:

1. $$SNR_{predicted} - SNR_{Desired} = 0 \rightarrow \frac{PT \cdot GT \cdot GR \cdot LFS \cdot LM}{N_0 \cdot B} - SNR_{Desired} = 0$$

P_T is the transmitter output power, L_M is the miscellaneous losses, L_{FS} is the free space path loss, G_T is the transmitting antenna gain, G_R is the receiving antenna gain **No** is noise energy, and **B** is the bandwidths. By using the two parameters, P_T and L_M, we achieve the power-saving goal. If the signal losses increase, the transmitter needs to increase signal strength and vice versa. This differential power supply saves satellite energy consumption.

LSTM Neural Network Prediction experiment across seasons

Section A: The experiment setup comprises an LSTM neural network system, a Matlab environment loaded with the code described in section 3.5, and 98 sample records described in section 3.6. We built the network using the LSTM method and created a tool that predicts SNR values for a future timeframe. The model succeeded in predicting the SNR sample for the next 1.5 seconds based on the data with a deviation of 1%, which is still reliable. We collected data from satellites, researched and explored optimal ways to build the deep neural network architecture of LSTM, and chose the parameters which reduce the function loss to a minimum. The bottom of Figure 5 depicts the LSTM neural network training process that outputs the predicted value for the next time frame. The top chart outlines the three-stage process, starting with data collection and the iterations between stage 2 and stage 3.

Preprints (www.preprints.org) | NOT PEER-REVIEWED | Posted: 2 December 2021 doi:10.20944/preprints202112.0031.v1

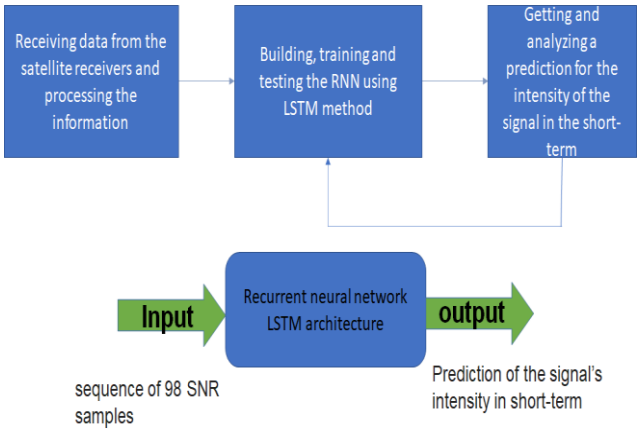

Figure 5. The proposed system.

The conceptual LSTM process, starting with all 98 samples, was reduced to 20 and finally to the resulting SNR value. We defined a hyper-parameters function, and with many empirical experiments, we found that the optimal parameters converged after four epochs. The parameters are a. Loss function: mean absolute error, b. Optimizer: Adam, c. Activation function: Tanh, d. Several epochs to saturation 4, 3 layers: 2 LSTM,1 Dense - First layer: 98 neurons, Second layer: 20 neurons, Last layer:1 neuron. Figure 6 depicts a chart of a one-month sampling experiment using a 10GHz frequency. It compares the predicted signal graph generated by the LSTM neural network [left] and the actual signal graph [right]. We can see that the two charts are very similar, with an average matching of 93%. We revealed similar results for the next four consecutive months, proving that the prediction accuracy depends on various behaviors across seasons.

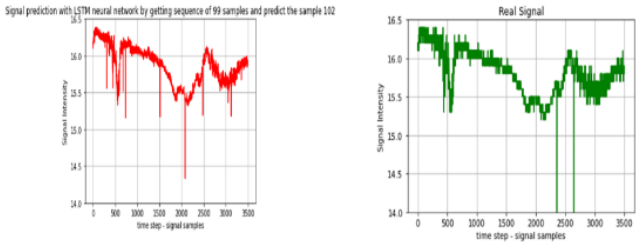

Figure 6. Comparison of the actual and predicted signal for one month.

Prediction experiment for 2.4-72GHz

We introduce the LSTM-ML process and compare the expected rain and fog attenuation levels to the accurate attenuation results executed over a broad spectrum of signal strengths, from 2.4GHz to 72GHz. The experiment began with training the LSTM system using 913 sample records collected. Figure 7 depicts the results achieved during the ML training process.

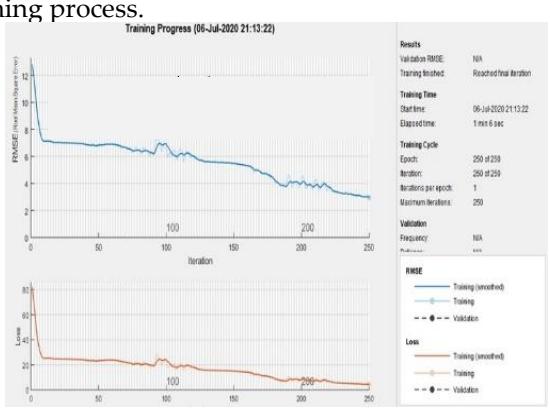

Figure 7. The attenuation levels derived from the training data compared to the actual data.

Preprints (www.preprints.org) | NOT PEER-REVIEWED | Posted: 2 December 2021 doi:10.20944/preprints202112.0031.v1

The top chart presents the trained attenuation levels derived from the training data. The bottom graph depicts the actual attenuation levels collected by the satellite. At this stage, we may assume that the LSTM-ML is appropriately calibrated and ready for the prediction process. We executed the same experiment with the same sampled data but with different signal strengths of 2.4, 10, 23, 48, and 72 GHz. Figure 8 depicts the results of the experiments performed for each of the five frequencies. For example, the blue and brick lines in the top frame represent the actual and predicted attenuation levels, respectively. The chart below depicts the differences between the two top charts. We can see the significant similarity between the two graphs. We can also see that all other frames demonstrate similar maps with neglected differences, excluding 72GHz, where we notice growing discrepancies at the beginning and the end.

In contrast, the smooth, while the brick chart (predicted results) has significant deviations in the map. We checked the training results, which look fine. Therefore, at this stage, we should limit the prediction of 72GHz to the middle part of the satellite orbit and leave the forecast for the edges for further investigation and adjustments to prevent these deviations. In summary, the prediction model works well for various frequencies but only partially for very high frequencies.

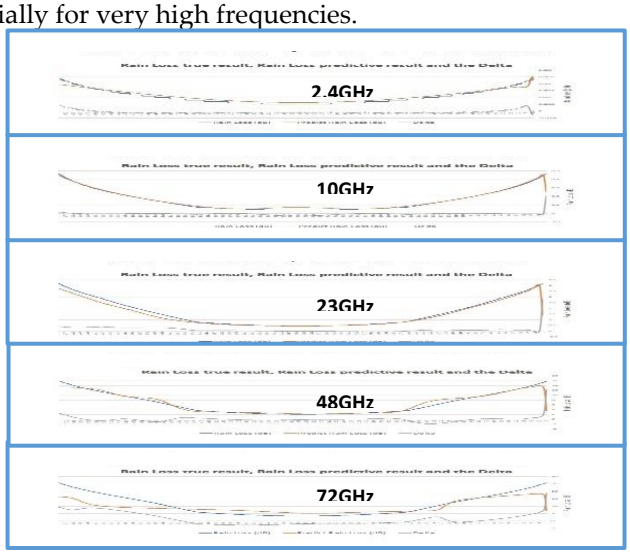

Figure 8: Comparison of the predicted data and the actual data

Section B: Predicting the signal attenuation after it goes through a type of construction requires several steps. In this section, we describe in detail the entire process. Following are the main process steps: Measuring the Building shadowing loss, Setting up the prediction model testbed, Constructing the database for the learners, Developing the predictive model, Training the learning system, and Aligning the Satellite signal strength.

3.1. Measuring Building shadowing loss

Building shadowing loss relates to the transmission loss through a building, as illustrated in Figure 9. Measurements have been formulated to calculate values of building shadowing loss to be used in planning frequency sharing between satellite to ground station. For example, the average loss through concrete/brick building for a frequency of 11 GHz. with vertical and horizontal polarization is 30.1 dB (Std. dev. 5.0) for V-Pol and 28.6 dB (Std. dev. 5.5) for H-Pol.

Preprints (www.preprints.org) | NOT PEER-REVIEWED | Posted: 2 December 2021 doi:10.20944/preprints202112.0031.v1

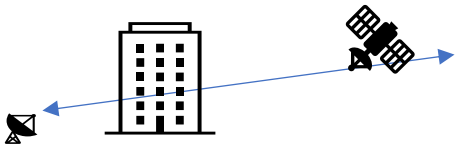

Figure 9: Building shadowing loss

3.2. Setting up the prediction model testbed

We performed our experiment on a building with a reinforced concrete shear wall structure. The following table is an example of the antenna setup features:

Transmitting antenna	**Omni-directional vertical polarization antenna**
Receiving antenna	Horn antenna with vertical polarization
Transmitter	Agilent E8267D signal generator
RF power amplifier	The output power in the test is set to 33 dBm
Receiver	Agilent N9030A signal analyzer

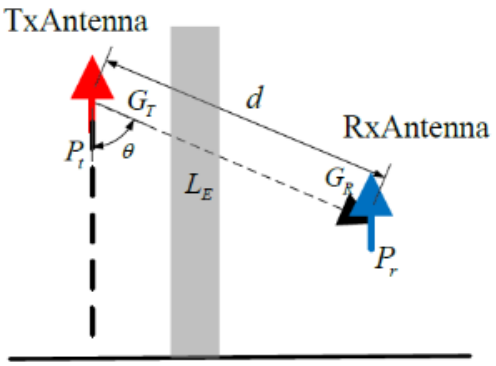

Figure 10: The relationship between the receiving and the transmitting antennas

Previous measurements show high dependency on construction material in determining the primary propagation mode and the amount of attenuation caused by the obstacle. Metal-based construction buildings generate the highest average signal attenuation, 35-40 dB. Concrete causes 25-35 dB, and wood 10- 25 dB. The transmission was the main propagation mode for wooden and concrete structures. At the same time, it was propagation by diffraction for metal, which increased from the corners towards the center of the building shadow. The attenuation due to diffraction increased in the order of 5.0 to 10.0 dB.

Preprints (www.preprints.org) | NOT PEER-REVIEWED | Posted: 2 December 2021 doi:10.20944/preprints202112.0031.v1

The formula for calculating the losses through the building

To better understand the meaning of the following formulas, Figure 10 describes the context of the elements used in the formulas presented in this section.

The free space loss formula is as follows:

$$L_{fs} = 32.45 + 20 \cdot log(d_{(m)}) + 20 \cdot log(f_{(GHz)}) \quad (1)$$

Where $\boldsymbol{d}$ is the distance defined in Fig. 2. $\boldsymbol{f}$ is the carrier frequency (GHz). Set transmitted power to be $\boldsymbol{Pt}$ (dBm) and received power to be $\boldsymbol{Pr}$ (dBm). The losses through the building are stated as $\boldsymbol{L_E}$, sending antenna gain, and receiving antenna gain in the transmission path are denoted as G_T and G_R, respectively.

Then we can get equation (2):

$$P_{t(dBm)} + \left(G_t - L_{fs} - L_E + G_r\right) = P_{r(dBm)} \quad (2)$$

And then, the losses through the building are inferred from equation (3).

$$L_E = \left(P_{t(dBm)} - P_{r(dBm)}\right) - L_{fs} + (G_t + G_r) \quad (3)$$

The Omni-dtional antenna used in the experiment is like a half-wave dipole antenna whose gain is 2.15 dB, and the normalized directivity function of the electric field of half-wave dipole antenna is presented by equation (4):

$$F(\theta) = sin(\theta) \quad (4)$$

From equation (4), we get equation (5):

$$G_t + G_r = 4.3 + 10 \cdot log([F(\theta)]^4) = 4.3 + 10 \cdot log(sin^4\theta) \quad (5)$$

The horn antenna is the receiving antenna in the building scenario, so the receiving antenna gain is appropriately considered.

3.3. Constructing the database for the learner

In this step, we used the collected data based on: (1) the building loss, (2) geometric calculations related to the location of the ground station and the height of the building, (3) and satellite orbits to build a learning database that will enable building loss prediction. The input data came from STK simulation, which links satellite orbit (time and angle) with channel orientation, and geometric calculations relating to a particular scenario. Table 2 depicts an example of the database record layout used for our experiment with a signal frequency of 72 GHz:

Table 2. Dataset records were used for our prediction experiment.

Time (LCLG)	Azimuth (deg)	Elevation (deg)	Range (km)	EIRP (dBW)	Xmtr Power (dBW)	Xmtr Gain (dB)	Xmtr EIRP Intensity (dBW/Sterad)	Atmos Loss (dB)	UrbanTerres Loss (dB)
24/6/2020 12:18:20	269.08	5	2092.57019	84.8873	30	126.7933	73.7783	17.4649	243.72
24/6/2020 12:18:21	269.082	5.048	2088.404155	84.7149	30	126.6204	73.6048	17.3154	243.09
24/6/2020 12:18:22	269.086	5.124	2081.780892	84.6428	30	126.4718	73.5434	17.0813	242.39
24/6/2020 12:18:23	269.09	5.201	2075.118827	84.5081	30	126.3504	73.475	16.8524	241.64
24/6/2020 12:18:24	269.094	5.278	2068.477073	84.3521	30	126.2628	73.3019	16.6285	241.02
24/6/2020 12:18:25	269.098	5.355	2061.836346	84.2634	30	126.1509	73.2396	16.4095	240.32
24/6/2020 12:18:26	269.102	5.432	2055.196461	84.1542	30	126.0643	73.114	16.1952	239.76
24/6/2020 12:18:27	269.106	5.51	2048.557434	84.102	30	125.9882	72.9149	15.9854	239.08
24/6/2020 12:18:28	269.11	5.588	2041.919281	83.91	30	125.8196	72.7792	15.7801	238.46
24/6/2020 12:18:29	269.114	5.666	2035.28017	83.8062	30	125.6888	72.697	15.579	237.76
24/6/2020 12:18:30	269.118	5.745	2028.645659	83.7767	30	125.6444	72.688	15.3821	237.21
24/6/2020 12:18:31	269.122	5.824	2022.010222	83.7702	30	125.5029	72.4907	15.1892	236.62
24/6/2020 12:18:32	269.126	5.903	2015.375724	83.5991	30	125.3556	72.3137	15.0002	236.06

This dataset will serve for training the deep learning system described in the next step. Above the table header is the source of each table column.

Preprints (www.preprints.org) | NOT PEER-REVIEWED | Posted: 2 December 2021 doi:10.20944/preprints202112.0031.v1

3.4. Developing the predictive model

For the prediction method, deep learning (DL) algorithm was used, with the following steps:

1). Accept the training and experiment dataset

As mentioned, Table 2 is an example of the training and experiment data set required as input to the predicting system. The label class in this case can be binary (e.g., **+1** (if attenuation = 0), **-1** (if attenuation ≠ 0)).

2). Execute the Prediction deep learning algorithm

The following notation demonstrates the prediction procedure in:

$$X_{m \times n,d,t} \rightarrow Y_{m^* \times 1,d,t+\Delta t} \ (train\ file) \quad (6)$$

$$X_{\tilde{m} \times n,d^*,t} \rightarrow Y_{\tilde{m}^* \times 1,d^*,t+\Delta t} \ (experiment\ file) \quad (7)$$

X represents samples of satellite data, with matrices size $m \times n$ produced at a specific date d and specific time t with class labels m^* produced for the same date d but with different time $t+\Delta t$). The trained classifier classified the experiment samples (made from latterly date d* and specific time t). Because the algorithm classifier labels for future times, it is a prediction of satellite attenuation.

Satellite data may vary according to both days and time (hours/min/sec). This section will denote by $X_{m\times n,d,t}$ a dataset of size m with n features, collected on day d and at time (hour/min/sec) t and by $Y_{m\times 1,d,t}$ the class labels associated $X_{m\times n,d,t}$. Therefore, the prediction problem is given a dataset $X_{m\times n,d,t}$ known for every time t to estimate $Y_{\tilde{m}\times 1,d+\Delta d,t+\Delta t}$, where Δd and Δt respectively define a variation of day and time (hour/min/sec).

The proposed estimation procedure then can be decomposed into four steps:

Collect two samples of data, $X_{m\times n,d,t}$ and $X_{m\times n,d,t+\Delta t}$, $\Delta t > 0$,

Compute the class labels $Y_{m\times 1,d,t+\Delta t}$,

Compute a new training set $Z_{m\times n+1,d}$, using $X_{m\times n,d,t}$, and $Y_{m\times 1,d,t+\Delta t}$ by concatenation, that is $Z_{m\times n+1,d} = [X_{m\times v,d,t}; Y_{m\times 1,d,t+\Delta t}]$

Collect the test set $X_{\tilde{m}\times n,d+\Delta d,t}$ ($\Delta d > 0$), and compute $Y_{\tilde{m}\times 1,d+\Delta d,t+\Delta t}$ using the machine learning algorithm on $Z_{m\times n+1,d}$ and $X_{\tilde{m}\times n,d+\Delta d,t}$

3.5. Training the learning system

In this stage, the learning system that predicts the channel attenuation is trained. Two different methods are used to find a faster and accurate process. We use the LSTM (long short-term memory) model using Python libraries. LSTM is an artificial neural network designed to recognize patterns in data sequences, such as numerical time series data emanating from sensors, stock markets, and government agencies. RNNs (recurrent neural networks) and LSTMs are different from other neural networks as they have a temporal dimension. Appendix 1 outlines the Python code.

3.6. Aligning the Satellite signal strength

The predicted signal-to-noise ratio (SNR) is sent back from the ground station to the satellite. The aim is to maintain a constant level of satellite link budget, which is conveyed by the desired signal-to-noise ratio level and may be different from the predicted signal-to-noise ratio level. We use the following model:

Preprints (www.preprints.org) | NOT PEER-REVIEWED | Posted: 2 December 2021 doi:10.20944/preprints202112.0031.v1

$$SNR_{predicted} - SNR_{Desired} = 0 \rightarrow \frac{P_T \cdot G_T \cdot G_R \cdot L_{FS} \cdot L_E}{N_0 \cdot B} - SNR_{Desired} = 0 \quad (8)$$

where P_T is transmitter output power, L_E is losses through the Building, L_{FS} is free space path loss, G_T is the transmitting antenna gain, G_R is the receiver antenna gain, No is noise energy, and B is the bandwidth.

By using the two parameters, P_T and L_E, we achieve this goal. If the losses through the building decrease, the transmitter output power needs to increase and vice versa.

The setup of the LSTM experiment

The experiment setup comprises an LSTM L, a Python environment loaded with the code described in the Appendix, and sample records described in section 3.5. We have built the network using the LSTM method and created a tool that predicts SNR values for a future timeframe. The model succeeded in predicting the SNR sample one second in advance, based on the samples with a loss of 1%, which is still reliable. We collected data from satellites, researched and explored optimal ways to build the deep neural network architecture of LSTM, and chose the parameters which reduce the loss function to a minimum. The bottom of Figure 5 depicts the LSTM training process where we load the input records to the LSTM neural network. The output is a predicted value for the next time frame (1 second). The top chart outlines the three-stage process encapsulated in the bottom graph and the iterations between stages 2 and 3.

The LSTM mechanism comprises several epochs, starting with the entire input samples, reducing to a smaller number, and reducing to one instance at the final stage.

In this work, we developed a hyper-parameters function, and with several empirical experiments, we identified the optimal parameters converged after four epochs. The parameters are a. Loss function: mean absolute error, b. Optimizer: "Adam", c. Activation function: “tanh”, d. Number of epochs to saturation: 4, 3 layers: 2 LSTM,1 Dense - First layer: 98 neurons, Second layer: 20 neurons, Last layer:1 neuron.

We used the LSTM process and compared the predicted building attenuation levels to the actual attenuation results executed over a wide variety of frequencies, from 2.4GHz up to 72GHz. The experiment started with training the LSTM system using 913 sample records from the STK satellite simulation connected to its corresponding earth station. Figures 11 to 16 depict the results of the experiments performed for each of the five frequencies. The average difference between the predicted results and the actual results is below 2%. It can be seen visually from the presented figures. The y-axis represents the signal loss through the building in dB. The x-axis represents times (from the moment the ground station discovers the satellite) in seconds or the satellite's angle (above the ground) in degrees. The blue and orange lines in the top frame represent the actual and predicted attenuation levels, respectively. We can see how close the two charts are and realize that all other figures demonstrate similar charts. We checked the training results, and they resemble the accurate results to a convincing extent.

Preprints (www.preprints.org) | NOT PEER-REVIEWED | Posted: 2 December 2021 doi:10.20944/preprints202112.0031.v1

The results are as follows:

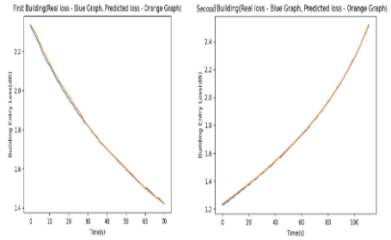

Figure 11: Prediction of building loss for 2.4Ghz

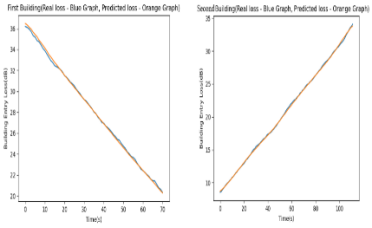

Figure 12: Prediction of building loss due to building at a frequency of 10Ghz

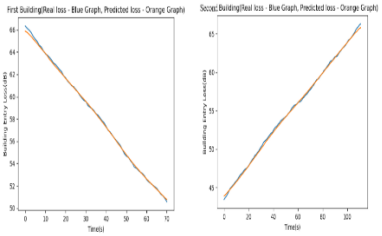

Figure 13: Prediction of building loss due to building at a frequency of 15Ghz

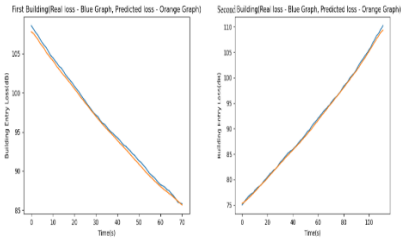

Figure 14: Prediction of building loss due to building at a frequency of 23Ghz

Preprints (www.preprints.org) | NOT PEER-REVIEWED | Posted: 2 December 2021 doi:10.20944/preprints202112.0031.v1

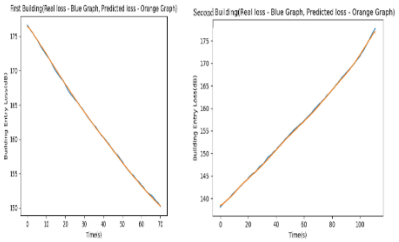

Figure 15: Prediction of building loss due to building at a frequency of 48Ghz

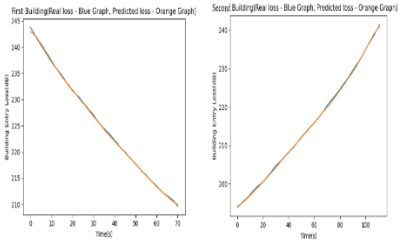

Figure 16: Prediction of building loss due to building at a frequency of 72Ghz

CONCLUSIONS AND FUTURE WORK

This research aimed to optimize the energy consumed by a satellite transmitter for proper propagation of microwave signals towards its associated ground station, enabling broadband communication. A signal between the satellite and the ground station suffers from attenuation caused by climatic phenomena and physical obstacles rounding the ground station. We proposed a prediction mechanism using LSTM neural networks. We collected and simulated data from the Genesis satellite and built a sampling dataset to serve as the training data loaded to the LSTM system. We executed the predicting scheme for various frequencies and independent setup with excellent predictions. We intend to improve the prediction further in future work and apply it to other obstacles causing signal attenuation and loss.

References

[1] Samad MA, Choi D-Y. Learning-Assisted Rain Attenuation Prediction Models. MDPI-*Applied Sciences*. 2020; 10(17):6017. https://doi.org/10.3390/app10176017

[2] .M. Kalaivaanan, A. Sali, R. S. A. Raja Abdullah, S. Yaakob, M. Jit Singh and A. M. Al-Saegh, "Evaluation of Ka-Band Rain Attenuation for Satellite Communication in Tropical Regions

[3] Isabelle Dahman, Philippe Arbogast, Nicolas Jeannin, and Bouchra Benammar, Rain attenuation prediction model for satellite communications based on the Météo-France ensemble prediction system PEARP, Nat. Hazards Earth Syst. Sci., 18, 3327–3341, 2018

[4] Golovachev Y, Pinhasi GA, Pinhasi Y. Atmospheric Effects on OFDM Wireless Links Operating in the Millimeter Wave Regime. *MDPI, Electronics*. 2020; 9(10):1598. Doi:10.3390.electronics.91058

[5] Boncho Bonev, Kliment Angelov, and Emil Altimirski, Experimental Estimation and Correction of the Methods for Radio Waves Attenuation Prediction in Rain, I C E S T 2012 28-30 JUNE, 2012,

[6] A. A. H. Budalal, M. R. Islam, K. Abdullah, and T. Abdul Rahman, "Modification of Distance Factor in Rain Attenuation Prediction for Short-Range Millimeter-Wave Links," in *IEEE Antennas and Wireless Propagation Letters*, vol. 19, no. 6, pp. 1027-1031, June 200.

[7] P Through a Measurement of Multiple Antenna Sizes," in *IEEE Access*, vol. 8, pp. 18007-18018, 2020.

[8] J. X. Yeo, Y. H. Lee and J. T. Ong, "Rain Attenuation Prediction Model for Satellite Communications in Tropical Regions," in *IEEE Transactions on Antennas and Propagation*, vol. 62, no. 11, pp. 5775-5781, Nov. 2014, DOI: 10.1109/TAP.2014.2356208

[9] Islam, R.M., Abdulrahman, Y.A. & Rahman, T.A. An improved ITU-R rain attenuation prediction model over terrestrial microwave links in a tropical region. *J Wireless Com Network* 2012, 189 (2012). https://doi.org/10.1186/1687-1499-2012-189

[10] M. N. Ahuna, T. J. Afullo and A. A. Alonge, Rain Attenuation Prediction Using Artificial Neural Network for Dynamic Rain Fade Mitigation, in *SAIEE Africa Research Journal*, vol. 110, no. 1, pp. 11-18, March 2019, DOI: 10.23919/SAIEE.2019.8643146

[11] Dalia Das, Animesh Maitra, Rain attenuation prediction during rain events in different climatic regions, Journal of Atmospheric and Solar-Terrestrial Physics, Volume 128, 2015, Pages 1-7, ISSN 1364-6826, https://doi.org/10.1016/j.jastp.2015.03.003.

[12] N Fadilah and R Pratama, Comparison of rain attenuation estimation in high frequency in Indonesia region for LAPAN communication satellite, IOP Conf. Series: Journal of Physics: Conf. Series 1130 (2018) 012036 DOI:10.1088/1742-6596/1130/1/012036

[13] Sakir Hossain and Atiqul Islam, Estimation of Rain Attenuation at EHF bands for Earth-to-Satellite Links in Bangladesh, International Conference on Electrical, Computer and Communication Engineering (ECCE), Feb. 16-18, 2017, Bangladesh

[14] T. Ngo, B. Kelley, and P. Rad, "Deep Learning-Based Prediction of Signal-to-Noise Ratio (SNR) for LTE and 5G Systems," 2020 8th International Conference on Wireless Networks and Mobile Communications (WINCOM), 2020, pp. 1-6, DOI: 10.1109/WINCOM50532.2020.9272470.

[15] P. Kazemi, H. Al-Tous, C. Studer and O. Tirkkonen, "SNR Prediction in Cellular Systems based on Channel Charting," 2020 IEEE Eighth International Conference on Communications and Networking (ComNet), 2020, pp. 1-8, DOI: 10.1109/ComNet47917.2020.9306087.

[16] S. H. A. Shah, M. Sharma, and S. Rangan, "LSTM-Based Multi-Link Prediction for mmWave and Sub-THz Wireless Systems," ICC 2020 - 2020 IEEE International Conference on Communications (ICC), 2020, pp. 1-6, DOI: 10.1109/ICC40277.2020.9148975.

[17] Tozer TC, Grace D: High-altitude platforms for wireless communications. Electronics & Communication Engineering Journal 2001, 13(3):127-137. 10.1049/ecej:20010303

[18] ITU-R Rec. P.1411-3: Propagation data and prediction methods for planning short-range outdoor radiocommunication systems and radio local area networks in the frequency range 300 MHz to 100 GHz. 2005.

[19] Stone W: Electromagnetic signal attenuation in construction materials. National Institute of Standards and Technology, Gaithersburg, Md, USA; October 1997.

[20] Baker-Jarvis J, Janezic MD, Riddle BF, et al.: Measuring the permittivity and permeability of lossy materials: solids liquids, building material, and negative index materials. National Institute of Standards and Technology, Gaithersburg, Md, USA; February 2005.

[21] Stavrou S, Saunders SR: Review of constitutive parameters of building materials. Proceedings of the 12th International Conference on Antennas and Propagation (ICAP '03), March-April 2003, Exeter, UK 1: 211-215.

[22] De Toledo AF, Turkmani AMD, Parsons JD: Estimating radio transmission coverage into and within buildings at 900, 1800, and 2300 MHz. IEEE Personal Communications 1998, 5(2):40-47. 10.1109/98.667944

[23] Martijn EFT, Herben MHAJ: Characterization of radio wave propagation into buildings at 1800 MHz. IEEE Antennas and Wireless Propagation Letters 2003, 2(1):122-125.

[24] Vogel WJ, Torrence GW: Propagation measurements for satellite radio reception inside buildings. IEEE Transactions on Antennas and Propagation 1993, 41(7):954-961. 10.1109/8.237628

[25] Oestges C, Paulraj AJ: Propagation into buildings for broadband wireless access. IEEE Transactions on Vehicular Technology 2004, 53(2):521-526. 10.1109/TVT.2004.823546

[26] Devasirvatham DMJ, Krain MJ, Rappaport DA, Banerjee C: Radio propagation measurements at 850 MHz, 1.7 GHz, and 4 GHz inside two different offices buildings. Electronics Letters 1990, 26(7):445-447. 10.1049/el:19900289

[27] Nobles P, Halsall F: Delay spread measurements within a building at 2 GHz, 5 GHz, and 17 GHz. Proceedings of the IEE Colloquium on Propagation Aspects of Future Mobile Systems, October 1996, London, UK 8/1-8/6.

[28] Report ITU-R, Compilation of measurement data relating to building entry loss (2015/05) ,

[29] Perez-Fontan, Fernando, et al. "Building entry loss and delay spread measurements on a simulated HAP-to-indoor link at S-band." EURASIP Journal on wireless communications and networking 2008 (2008): 1-6.

[30] Plets, David, et al. "Simple indoor path loss prediction algorithm and validation in living lab setting." *Wireless Personal Communications* 68.3 (2013): 535-552.

[31] D. Micheli, Fabio Santoni, and Andrea Delfini, "Measurement of Electromagnetic Field Attenuation by Building Walls in the Mobile Phone and Satellite Navigation Frequency Bands," IEEE Antennas and Wireless Propagation Letters 14:1, December 2014, DOI:10.1109/LAWP.2014.2376811

[32] Al-Hourani and I. Guvenc, "On Modeling Satellite-to-Ground Path-Loss in Urban Environments," in IEEE Communications Letters, vol. 25, no. 3, pp. 696-700, March 2021, DOI: 10.1109/LCOMM.2020.3037351.